Chalcogenide Letters Vol. 12, No. 6, June 2015, p. 301 - 312

# INFLUENCE OF HUBBARD COEFFICIENT ON THE STRUCTURAL, ELECTRONIC, MAGNETIC AND OPTICAL PROPERTIES OF Mn/Fe CODOPED ZnS

A. ABBAD[a*], H. A. BENTOUNES[a], W. BENSTAALI[b], S. BENTATA[b], B. BOUADJEMI[b]

[a]*Signals and Systems Laboratory (LSS), Faculty of Sciences and Technology, BP227, Abdelhamid Ibn Badis University, Mostaganem (27000) Algeria*

[b]*Laboratory of Technology and Solids Properties, Faculty of Sciences and Technology, BP227, Abdelhamid Ibn Badis University, Mostaganem (27000) Algeria*

We have investigated the structural, electronic and magnetic properties of substitutional iron and manganese transition metal impurities in wurtzite ZnFeMnS by employing the ab-initio method. Calculations were performed by using the full potential linearized augmented plane wave (FPLAPW) method within the framework of spin-polarized density functional theory (DFT). The electronic exchange correlation energy is described by generalized gradient approximation GGA and GGA+U (where U is the Hubbard correction). The GGA+U method is applied to iron 3d states. We have calculated the lattice parameters, bulk modulus, the first pressure derivative of the bulk modulus and the cohesive energies. The calculated densities of states presented in this study identify the half-metallic behavior of ZnFeMnS when we use the GGA+U scheme with spin up channels metallic and spin down ones semiconducting. The half-metallicity depends strongly on the value of Hubbard coefficient U until the critical value of 8 eV. Furthermore, we have calculated optical properties, and found interesting results.

(Received May 8, 2015; Accepted June 12, 2015)

*Keywords:* Semiconductors; First Principle calculations; half-metallic; Magnetic properties; Optical properties

## 1. Introduction

Recently, diluted magnetic semiconductors (DMSs) have gained much attention due to the possibility of having magnetic properties. The DMS are III–V, II–VI, II–IV or IV–VI alloys in which cations are randomly substituted by the magnetic ions from the series of transition metals (such as Cr, Mn, Fe, Co or Ni). Research into diluted magnetic semiconductors (DMSs) has been motivated due to the opportunity of manipulating the electron spin in semiconducting devices as the base for the applications of spintronics [1, 2], which is the potential second-generation electronics, that focuses on the transmission of both charge and spin of electrons [3, 4]. It has additional extensive application foreground than microelectronics (the first generation electronics that only studies charges of electrons). More recently, there has been increasing interest in the spintronic materials, especially the half-metallic ferromagnets (HMFs) which have a 100% spin-polarization at the Fermi level. The concept of a HMF was introduced by de Groot et al. [5]. So far, there have been so many researches, both theoretically and experimentally, to find new half-metallic ferromagnets. Some of the materials that are approved to be half-metal theoretically or experimentally are Heusler compounds [6- 12], ferromagnetic metallic oxides [13-19], dilute magnetic semiconductors [20- 26] and zincblende transition-metal pnictides and chalcogenides [27- 31].

*Corresponding author: am.ben@voila.fr

Zinc Sulphide (ZnS) is an important II–VI compound semiconductor with potential applications in electronics and optoelectronics because of its wide direct band gap (3.7 eV). It has attracted great attention for its potential applications in electronics and optoelectronics [32- 36]. Many researches indicate that room temperature DMS could be achieved in ZnS by using proper dopants, such as Fe [37], Co [38] and Cu [39, 40]. Moreover, studies found that codoping (doping host simultaneously with two different TM impurities) is another effective route to achieve ferromagnetism. Computations within the density-functional theory (DFT) have been proven as a powerful method to understand the structural, magnetic, optical and electronic properties of semiconductors. However, calculations based on DFT that employ a local spin density approximation (LSDA) or a generalized gradient approximation (GGA) for the exchange and correlation potentials do not described adequately the electronic and magnetic structure of materials that contain 3d or 4f states. Furthermore, these schemes, generally underestimate the band gap values of semiconductors and insulators in relation to experimental values [41]. Among the methods proposed, the method yielding accurate electronic structure, magnetic properties, and band gaps is LSDA+U or GGA+U [42], where U is on-site Coulomb interaction and is applied to the correlated and localized 3d or 4f electrons in the transition and rare-earth metal compounds.

In a recent study, we have found that ternary ZnMnS may be an unsuitable material for applications in spintronics [43], so in the present work, we have performed first principle calculations on the structural, electronic, magnetic and optical structure of Fe/Mn co-doped wurtzite ZnS using the generalized gradient approximation (GGA) plus optimized effective Hubbard parameter U (GGA+U) within the framework of density functional theory (DFT), to search for half-metallic ferromagnets based ZnS and compare the obtained results with those calculated by using standard GGA.

## 2. Calculation

Electronic structure calculations were performed using the self-consistent full-potential linearized augmented plane wave (FPLAPW) method [44] implemented in WIEN2K code [45, 46] within the density functional theory (DFT). The Perdewe Burkee Ernzerhof generalized gradient approximation (GGA) [47] was used for the exchange correlation correction. In this method the space is divided into non-overlapping muffin-tin (MT) spheres separated by an interstitial region. We have used a structure of 32 atoms, where two atoms Zn are substituted by one atom Fe and one atom Mn for the quaternary compound. The basis functions are expanded into spherical harmonic functions inside the muffin-tin sphere and Fourier series in the interstitial region. The convergence of the basis set was controlled by a cutoff parameter $R_{mt}K_{max}$ =7.5 where $R_{mt}$ is the smallest of the MT sphere radii and $K_{max}$ is the largest reciprocal lattice vector used in the plane wave expansion. The cutoff energy, which defines the separation of valence and core states, was chosen as -7 Ry. In these calculations, we neglected the effect of spin orbit coupling. For the Brillouin zone (BZ) integration, the tetrahedron method with a 74 special k points in the irreducible wedge (200 k-points in the full BZ which corresponds to a mesh of 7*7*3) was used to construct the charge density in each self-consistency step.

## 3. Results and discussions

### 3.1 Structural properties

In the supercell used, two Zn atoms are replaced with one Mn and one Fe atom. We considered four possible configurations with different spatial position of TM atoms, named configuration I, configuration II, configuration III and configuration IV. After relaxation, the geometry changed very little due to the small difference in atomic radius of the transition metal atoms and Zn atom. The optimized structures are plotted in Fig. 1(a), (b), (c) and (d). In configurations I and II, the FM state is lower in energy than the AFM state. Our calculations give positive values of the total energy difference $\Delta E=\Delta E_{AFM}-E_{FM}$; thus, ZnFeMnS is stable in the FM

phase for the two cases cited. Also the formation energy $E_f$ was calculated, when the distance of the two TM atoms was smaller than 4 Å in configuration I, the magnetic coupling between the Mn and Fe atoms is long-ranged (table. 01), for this configuration (ground state), we have plotted in Fig. 02 the total energy of quaternary ZnFeMnS as a function of the unit cell volume using GGA.

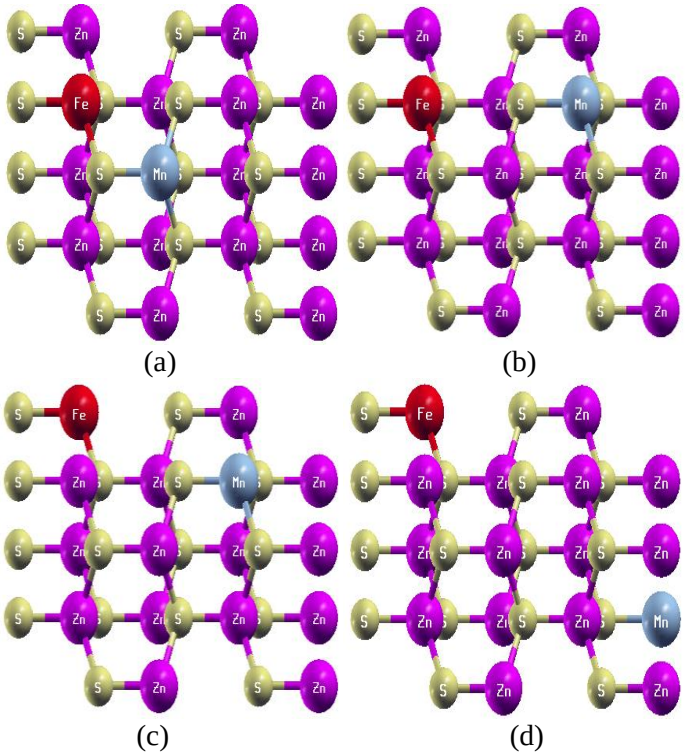


*Fig.1: Side-view of Fe/Mn codoped ZnS. The green, purple, red, and blue balls represent S, Zn, Fe, and Mn atoms, respectively. (a) Configuration (I), (b) Configuration (II), (c) Configuration (III) and (d) Configuration (IV).*

*Table1. Distance between Mn and Fe atoms ($d_{Mn-Fe}$ in Å) and energy difference (ΔE in eV) of the Mn/Fe codoped ZnS for the four configurations.*

| Configuration | $d_{Fe-Mn}$ | ΔE |
|---|---|---|
| I | 3.86 | 2.95 |
| II | 6.33 | 1.10 |
| III | 7.40 | -0.35 |
| IV | 11.16 | -0.12 |

The calculated lattice constants (a and c), bulk modulus (B), the pressure derivative of bulk modulus ($B_0$), for ZnFeMnS using standard GGA and GGA+U, are obtained according to Murnaghan's equation of state [48] and by fitting the total energy versus volume. The results obtained are summarized in Table 2. For GGA+U calculation, four different values of U are used (4, 6, 8 and 10 eV). The cohesive energies of this compound displayed also in Table 2 are calculated from the difference between the total atomic energies of Zn, S, Fe and Mn atoms and the minimum energy of bulk compound.

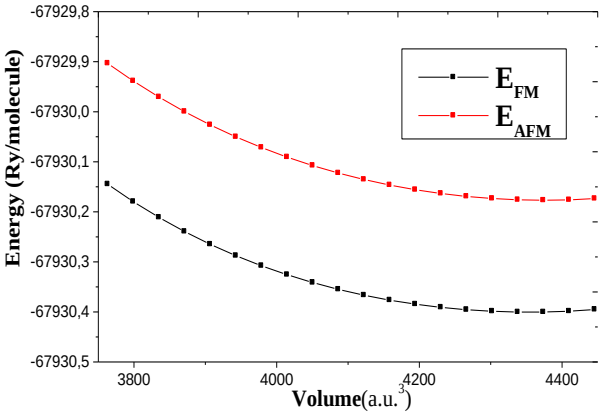


*Fig.2: The total energy of quaternary ZnFeMnS as a function of the unit cell volume for: both configurations Ferromagnetic (FM) and Anti-Ferromagnetic (AFM) phases using GGA in configuration (I).*

*Table2. Calculated resultants: equilibrium lattice parameters: a(Å), c (Å), bulk modulus B (GPa), its pressure derivative ($B_0$), cohesive energy (eV) and the band gap $E_g$ (eV)of Fe/Mn codoped ZnS obtained with GGA and GGA+U.*

| | a | c | B | $B_0$ | $E_g$ | $E_{coh}$ |
|---|---|---|---|---|---|---|
| GGA | 3.8379 | 6.3315 | 67.93 | 4.84 | 0.78 | -7.13 |
| U= 4eV | 3.8430 | 6.3399 | 64.83 | 4.86 | 1.11 | -6.95 |
| U= 6eV | 3.8488 | 6.3496 | 60.49 | 3.78 | 2.01 | -6.89 |
| U= 8eV | 3.8500 | 6.3515 | 61.14 | 4.21 | 2.22 | -6.83 |
| U= 10eV | 3.8524 | 6.3555 | 63.50 | 4.96 | 2.22 | -6.78 |

The calculated a, c, B, and $B_0$ using GGA+U depend on the U values. To reveal the dependence, the calculated a, c, B and the band gap Eg, as a function of U is shown in Fig. 03. We can notice that the calculated lattice parameters; a and c of ZnFeMnS by GGA+U, increase as U increases, but the cohesive energy $E_{coh}$ decreases. However, the calculated bulk modulus B shows a different trend. It, at first, decreases as U increases. Once the U reaches a critical value (8 eV), the calculated B increases. For the same value of U, the band gap remains constant. It is important to notice that there are no data available in the literature for possible comparison.

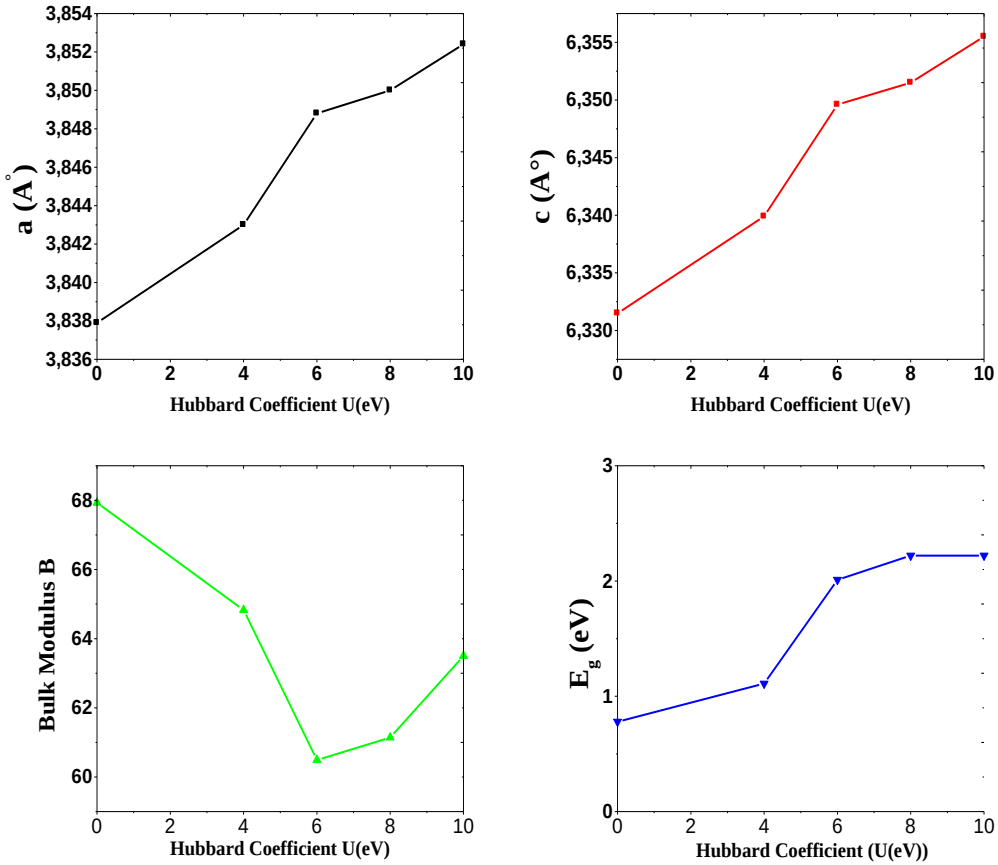


*Fig.3. Calculated lattice parameters a and c, the bulk modulus B and the band gap Eg, as a function of U.*

### 3.2 Electronic and magnetic properties

In order to understand clearly the electronic structure and magnetic properties of quaternary ZnFeMnS with wurtzite structure, its total and partial density of states (DOS) are given in Figs. 4 and 5 at their respective equilibrium lattice parameters. We can see from Fig. 4 (a), that majority spin electrons exhibit semiconducting nature, whereas minority spin electrons show metallic behavior, which keeps a fully spin-polarization of the states at the Fermi level. The total DOS around the Fermi level comes mainly from the Fe d and the S p electrons. However, from the density of states, we can see that, the states around Fermi level are isolated and the valence band and conduction one, are well separated, consequently, we can consider that the GGAis not enough to reproduce the half metallic behaviour on this compound. This is why, we have introduced the GGA+U approach, which properly describes the localization nature of d electrons and shows an energy gap comparable to the experimental data. The spin-dependent densities of states (DOSs) of ZnFeMnS are presented in Fig. 4(b, c, d and e). It shows a half metallic behavior with the majority of spin is metallic, whereas the minority spin is semiconducting for the four values of U.

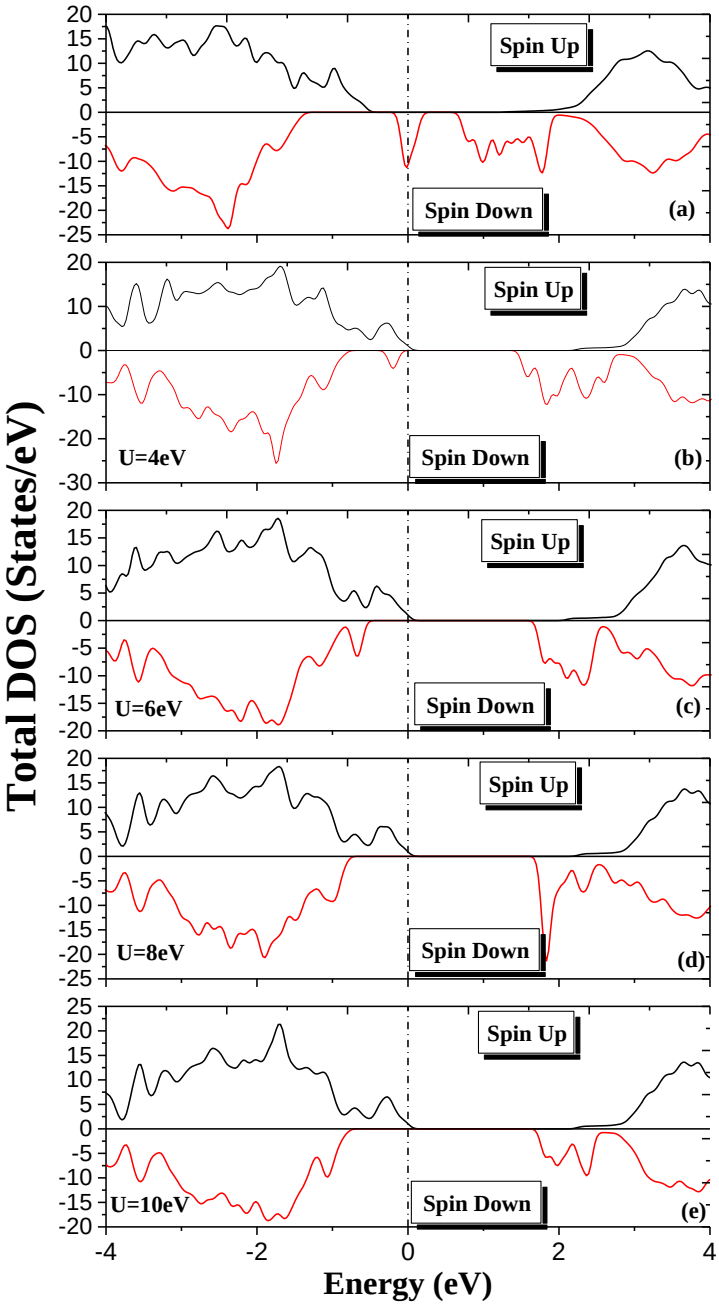


*Fig.4. Total density of States of ZnFeMnS using GGA and GGA+U. Fermi level is set to zero.*

The partial density of states (PDOS) using GGA+U was calculated to understand the spin polarization of Mn and Fe codoped zinc sulfide. For demonstration, the PDOS of this compound is shown in Fig. 4 (b, c, d and e) and reveals interesting remarks. It illustrates that the peak near Fermi level in Fig. 4(a) which was due to the Fe d orbitals, is shifted to negative energies and enters in the valence band, and as U increases, it becomes less important until it begins to disappear completely after the critical value of 8eV. The valence band crosses the Fermi level, resulting in p-type conductivity and the states responsible for this crossing are Mn d with a very little contribution of anion p states. For U= 4 eV, we can notice also that electronic bands shown in the lower part of conduction band in electronic structure are mainly formed by a significant hybridization between Fe d and Mn d electrons. However, as U increases, this hybridization decreases and the Fe d bands are pushed up to higher energies. The overall nature of ZnFeMnS is half-metallic, which is much appreciated for spintronic applications as diluted magnetic

semiconductors, and the electronic structure of this compound is very sensitive to on-site Coulomb interaction U.

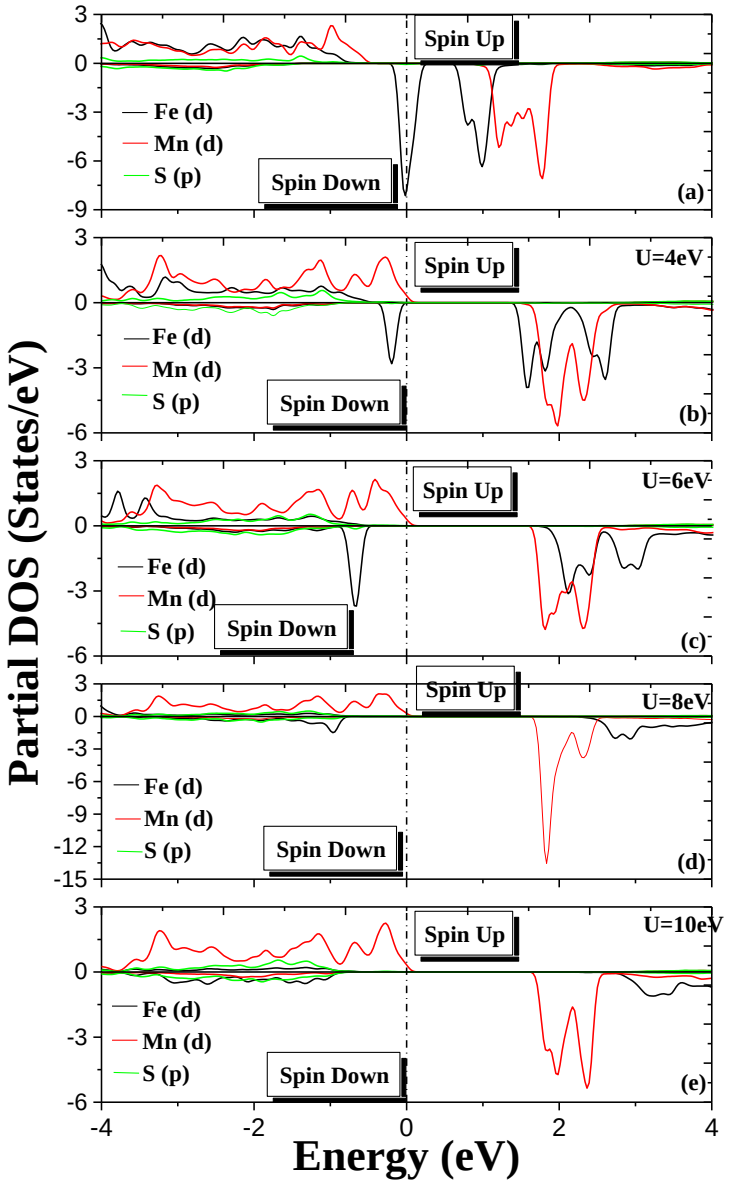


*Fig.5:Partial density of States of ZnFeMnS using GGA. Fermi level is set to zero.*

The calculated total and local magnetic moments per TM atom within the muffin-tin spheres as well as in the interstitial sites for ZnFeMnS are given in Table 3. Due to unoccupied TM 3d states, permanent local magnetic moments are produced in these materials. The results show that the total magnetic moments generally come from the TM ions with a little contribution of Zn and S sites whose magnetic moments are parallel to the TM ions. It can be seen from Fig. 05 that there is hybridization between S p states and the TM 3d states and this p–d hybridization decreases the total magnetic moments of the TM atoms from its free space charge value and generates a small local magnetic moments on the non-magnetic Zn and S atoms. The calculated total magnetic moment of ZnFeMnS compound is still 9 $\mu_B$, for GGA and GGA+U, and Hubbard coefficient doesn't affect $\mu_t$; however as U increases, the interstitial magnetic moment decreases and iron magnetic moment increases which maintains $\mu_t$ invariable. The calculated integer magnetic moment of the ZnFeMnS compound, which indicates stability of half-metallic behavior, follows the Slater-Pauling rule. According to the Slater-Pauling rule [49], the total magnetic

moment of the system is expressed as Mt = Zt-24, where Zt is the number of valence electrons, (Zn, Fe, Mn, and S atoms have twelve, eight, seven and six valence electrons, respectively).

*Table3.Calculated Magnetic Moments for several sites of the Fe/Mn codoped ZnS with: GGA and GGA+U Approximations.*

| | $\mu_{interstitial}$ | $\mu_{Fe}$ | $\mu_{Mn}$ | $\mu_{Zn}$ | $\mu_{S}$ | $\mu_{Tot}$ |
|---|---|---|---|---|---|---|
| GGA | 1.51 | 3.13 | 3.86 | 0.01 | 0.05 | 9 |
| U= 4eV | 1.48 | 3.33 | 3.86 | 0.01 | 0.03 | 9 |
| U= 6eV | 1.39 | 3.42 | 3.87 | 0.01 | 0.03 | 9 |
| U= 8eV | 1.35 | 3.49 | 3.86 | 0.01 | 0.03 | 9 |
| U= 10eV | 1.31 | 3.56 | 3.86 | 0.01 | 0.03 | 9 |

During the past years, numerous theoretical studies have been proposed to clarify the mechanism for ferromagnetism in diluted magnetic semiconductors. Here, we suppose p–d hybridization mechanism. According to Zener's p–d hybridization mechanism [50, 51], as the dopant adds partially occupied states into the gap of the host semiconductor, the FM state is reached by energy gain from band broadening. At the same time, due to the strong hybridizations between the Mn and its neighbouring anions S, the neighbouring anions are spin-polarized and coupled ferromagnetically with manganese.

### 3.3 Optical properties

The dielectric function $\varepsilon$ ($\omega$) of an anisotropic material is a complex, symmetric, second-order tensor. The imaginary part $\varepsilon_2$ ($\omega$) of the dielectric tensor is directly related to the optical absorption spectrum of the material, and it can be computed from knowledge of the electronic band structure of a solid.

Direct calculations of the imaginary part $\varepsilon_2$ ($\omega$) of the dielectric function are accessible in Wien2k code by evaluating the matrix elements of the electric dipole operator between the occupied and unoccupied electronic states in the valence band (VB), and in the conduction band (CB), respectively. The real and imaginary parts of the dielectric function $\varepsilon_1$ ($\omega$) and $\varepsilon_2$ ($\omega$); respectively, are then obtained from the Kramers–Kronig transform. The knowledge of the real and imaginary parts of dielectric function permits the calculation of the other optical coefficients, like the reflectivity, the refractive index, the absorption coefficient and the energy loss.

The calculated absorption coefficients for ZnFeMnS as a function of the incident radiation energy, by the GGA and GGA+U approaches, are shown in Fig. 6. The absorption is characterized by many broad absorption bands above the absorption threshold, which can be interpreted on the basis of the total DOS (Fig. 3 and 4) and interband transitions. For GGA and from the figure, we can notice the existence of an important peak in the region of low energies. This peak is generated by the presence of iron impurities according to the DOS. After the introduction of U Hubbard coefficient we can see a drastic change in optical absorption spectrum. Strong light absorption occurs in visible spectrum. For U=4eV, the absorption is increased and blue-shifted, also the peak in low frequencies has disappear for the different values of U. From the absorption spectra and the PDOS (Fig. 5), the enhanced visible light absorption of ZnFeMnS is attributed to the creation of impurity states in the band gap. With increasing U, we can see that optical absorption decreases again and is red-shifted compared to U=4eV, after the critical value of U=8eV, the curves, remain unchanged, so we can conclude that after a certain value, Hubbard coefficient does not affect optical properties but they are enhanced comparing to GGA.

The maximum value of absorption coefficient for GGA is 201, $7*10^4$ $cm^{-1}$, 235. $3*10^4$ $cm^{-1}$ for U=4eV, 217. $7*10^4$ $cm^{-1}$ for U=6 eV and 209. $6*10^4$ $cm^{-1}$ for U= 8 and 10 eV. The results obtained confirm that ZnFeMnS has significant absorption in large range of photon energies, and consequently, it is suitable for device applications in the major parts of the spectrum and may be used as material for photovoltaic cell and photo-catalyst.

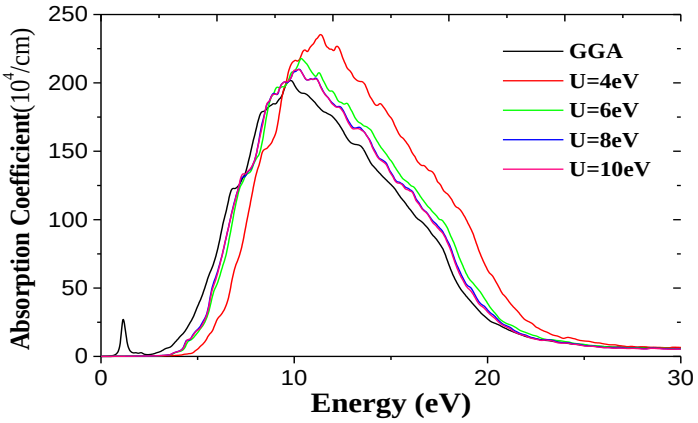


*Fig.6.Absorption coefficient of ZnMnS and ZnFeMnS.*

In Fig. 7 we plot the reflectivities of quaternary ZnFeMnS from the infrared spectral region to the ultraviolet. We find the same trend found in the absorption. For the GGA, we see that the reflectivity is very close to 43 % in the infrared, due to the peak caused by the absorption peak which we have related to Fe impurities. The maximum of reflectivity occurs in the energy range 5 - 17 eV and arises from inter-band transition. For GGA+U the minimum of reflectivity occurs in the energy range 1- 5 eV and is probably due to the collective plasma resonance. The depth of the plasma resonance can be determined by the imaginary part of the dielectric function [52]. It is also found that the shapes of the four curves for are very similar, and from the critical value of U=8eV, the curves are superposed. The peaks of reflectivity curve are shifted to higher energy side comparing to the GGA.

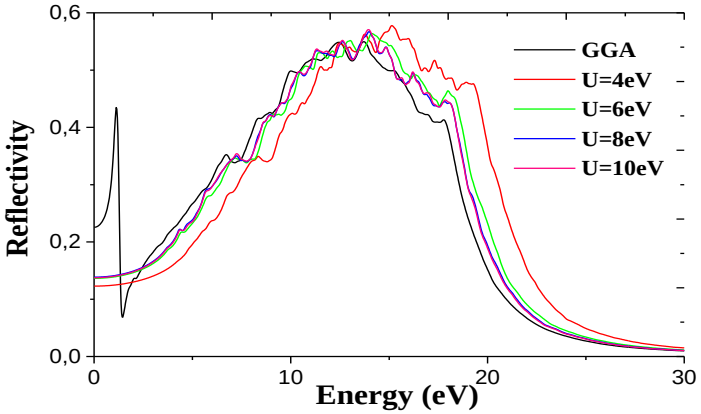


*Fig.7. Frequency dependent reflectivity of ZnFeMnS.*

The calculated refractive index of ZnFeMnS using GGA and GGA+U is presented in Fig. 8. A broad spectrum over a wide energy and frequency is noted. We can notice the same trend as for the other optical properties studied before. It is clear from the figure that the refractive index of the material is blue-shifted with the increase of U coefficient. For GGA, a maximum can be observed in the form of a bump in the spectrum at a particular energy. For GGA and GGA+U, and at intermediate energies a few bumps appear and then the curves vanish at higher energies.

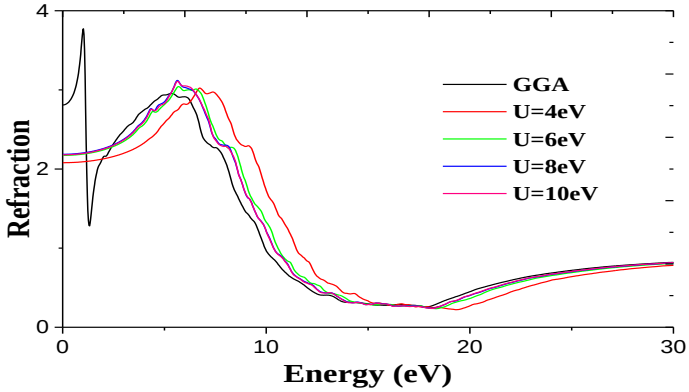


*Fig.8. Refraction of ZnFeMnS.*

## 4. Conclusions

In summary, the structural, electronic, magnetic and optical properties of Mn/Fe codoped ZnS were studied in terms of first-principle calculation within GGA+U and GGA approximations for the exchange and correlation potential. We found a shifting majority as well as minority Fe d bands away from Fermi level when GGA + U is used, leading to a better representation for the DOS at the Fermi level. Electronic structures indicate that ZnFeMnS is p-type half-metallic FM semiconductor at equilibrium lattice constants, with a magnetic moment of 9 $\mu_B$ withp–d hybridization mechanism is responsible for the ferromagnetism. The magnetic moment mainly comes from partially filled d orbitals of Fe and Mn. The origin of half-metallicity is due to the appearance of Mn d and S p bands near the Fermi level.The electronic structure and structural peoperties of this compound are very sensitive to on-site Coulomb interaction U. The half-metallicity of ZnFeMnS and the large positive value of total energy difference (ΔE), make this compound as a good candidate for spintronic applications. Furthermore, we have computed the reflectivity, the absorption coefficient and the refractive index of ZnFeMnS in a wide spectral range. For GGA+U the absorption is increased and blue-shifted comparing to the GGA, also the peak in low frequencies (in GGA) has disappear for the different values of U and for all optical properties studied. The compound has significant absorption in large range of photon energies, and consequently, it is appropriate for device applications in the major parts of the spectrum (visible and ultraviolet).

## References

[1] Dietl T, Ohno H, Matsukura F, Cibert J, Ferrand D. Science **287**, 1019 (2000).
[2] L.H. Liu, L.H. Yu, Intermetallics**5 7**, 139 (2015).
[3] M. Katsnelson, V. Y. Irkhin, L. Chioncel, A. Lichtenstein, R. De Groot, Rev. Mod.Phys. **80**,315 (2008).
[4] P. Liang , Y. Liu , X. H. Hu , L. Wang , Q. M. Dong , X. F. Jing, Journal of Magnetism and Magnetic Materials **355**,295(2014).
[5] R.De Groot, F. Mueller, P.VanEngen,K. Buschow, Phys.Rev.Lett. **50**,2024 (1983).
[6] X. Q. Chen, R. Podloucky, P. Rogl. J ApplPhys **100**,113901 (2006).
[7] N. Kervan, S. Kervan.Intermetallics **24**, 56 (2012).
[8] H.C. Kandpal, G.H. Fecher, C. J. Felser, J Phys D. ApplPhys **40**, 1507 (2007).
[9] Liu GD, Dai XF, Lui HY, Chen JL, Li YX, Xiao G, et al. Phys Rev B **77**, 14424 (2008).
[10] K. Özdogan, I. Galanakis, J. Mag. Mag Mater **321**, L34 (2009).
[11] V. Sharma, A.K. Solanki, A. Kashyap, J. Mag. Mag Mater **322**, 2922 (2010).
[12] H. Zenasni, H.I. Faraoun, C. Esling, Journal of Magnetism and Magnetic Materials **333**,162 (2013).
[13] F. Samir Matar, Journal of Magnetism and Magnetic Materials, 368, **105** (2014).

[14] A. Faisal Al-Agel, Esam Al-Arfaj, A. Ahmed Al-Ghamdi, YaroslavLosovyj, Lyudmila M. Bronstein, Waleed E. Mahmoud, Journal of Magnetism and Magnetic Materials **360**, 73 (2014).
[15] N. Hamdad, Superlattices and Microstructures**76**,425 (2014).
[16] A. F.Lamrani, M. Ouchri, M. Belaiche, A. El Kenz, M. Loulidi, A. Benyoussef, Thin Solid Films, **570**,45 (2014).
[17] Z. Szotek, W.M. Temmerman, A. Svane, L. Petit, G.M. Stocks, H. Winter, J Mag Mag Mater **1816**,272 (2004).
[18] W. Song, J. Wang, Z. Wu, ChemPhys Lett **482**, 246 (2009).
[19] S. Lv, H. Li, D. Han, Z. Wu, X. Liu , J. Meng, J. Mag. Mag. Mater **323**, 416 (2011).
[20] Y. Zhang, W. Liu, H. Niu, Solid State Commun**145**, 590 (2008).
[21] Y. Saeed, S. Nazir, A. Shaukat, A.H. Reshak, J. Mag. Mag Mater **322**, 3214 (2011).
[22] S. Kervan, N. Kervan, Journal of Magnetism and Magnetic Materials **382**, 63 (2015).
[23] S. Hardev Saini, M. Singh, A.H. Reshak, K. Manish Kashyap, Journal of Magnetism and Magnetic Materials **331**,1 (2013).
[24] A. Suneela, B. Amin, A. Iftikhar, M. Maqbool, R. Ahmad, M. Haneef, N. Ikram, Current Applied Physics **12**, 184 (2012).
[25] M. El Amine Monir, H. Baltache, R. Khenata, G. Murtaza, SikanderAzam, A. Bouhemadou, Y. Al-Douri, S. Bin Omran, R. Ali, Journal of Magnetism and Magnetic Materials **378**,41 (2015).
[26] X.F. Li, J. Zhang, B. Xu, K.L. Yao, Journal of Magnetism and Magnetic Materials **324(4)**, 584 (2012).
[27] I. Galanakis, P. Mavropoulos, PhysRev B **67**,104417 (2003).
[28] Y.Q. Xu, B.G. Liu, D.G. Pettifor, Physica B **1117**, 329 (2003).
[29] K.L. Yao, G.Y. Gao, Z.L. Liu, L. Zhu, Solid State Commun**133**, 301 (2005).
[30] K.L. Yao, G.Y. Gao, Z.L. Liu, L. Zhu, Y.L. Li, Physica B **366**, 62 (2005).
[31] X.F. Ge, Y.M. Zhang, Journal of Magnetism and Magnetic Materials **321**,198 (2009).
[32] K. Deepa, K.C. Preetha, K.V. Murali, A.C. Dhanya, A.J. Ragina, T.L. Remadevi, Optik–International Journal for Light and Electron Optics, **125(19)**, 5727 (2014).
[33] Z. Chen, X.X. Li, G. Du, Q. Yu, Bo. Li, X. Huang, Ceramics International **40(8)**, 13151 (2014).
[34] S. Zhou, Y. Li, Z. Chen, X.X. Li, N. Chen, G. Du, Ceramics International **39(6)**, 6763 (2013).
[35] R. Viswanath, H.S. BhojyaNaik, G.S. Yashavanth Kumar, P.N. Prashanth Kumar, K.N. Harish, M.C. Prabhakara, Spectrochimica Acta Part A: Molecular and Biomolecular Spectroscopy**125**, 222 (2014).
[36] J. Yuvaloshini, Ra. Shanmugavadivu, G. Ravi, Optik - International Journal for Light and Electron Optics, **125(6)**, 1775 (2014).
[37] S. Sambasivama, D. P.Josephb, D. R.Reddya, B.K. Reddya, C.K. Jayasankara, Mater. Sci. Eng. B **150(2)**, 125 (2008).
[38] S.P. Patel, J.C. Pivin, A.K. Chawla, R. Chandra, D. Kanjilal, L. Kumar, J. Magn. Magn. Mater. **323(22)**, 2734 (2011).
[39] C.W. Zhang, S. S. Yan, J. Appl. Phys. **107(4)**, 043913 (2010).
[40] H.Y. Yan, Y.Q. Li, Y.R. Guo, Q.G. Song, Y.F. Chen, Phys. B: Condens. Matter **406(3)**, 545 (2011).
[41] A.J. Cohen, P. Mori-Sanchez, W. Yang, Science **321**, 792 (2008).
[42] V.I. Anisimov, J. Zaanen, O.K. Andersen, Phys Rev B **44**, 44943 (1991).
[43] A. Abbad, S. Bentata, H.A. Bentounes, W. Benstaali, B.Bouadjemi, Material Science in Semiconductor Processing **16**, 576 (2013).
[44] O.K. Andersen, Phys. Rev. B 12 (1975) 3060.
[45] K. Schwarz and P. Blaha Computational Materials Science **28**, 259 (2003).
[46] P. Blaha, K. Schwarz, G. K. H. Madsen, D. Kvasnicka, J. Luitz, Techn. Universitat Wien, Austria, 2001.
[47] J.P. Perdew, A. Ruzsinszky, I.G. Csonka, O.A. Vydrov, G.E. Scuseria, L.A. Constantin, X. Zhou, K. Burke, Phys.Rev.Lett**100**, 136406 (2008).
[48] F.D. Murnaghan, Proc. Natl. Acad. Sci. USA **30**, 5390 (1944).
[49] T. Graf, C. Felser, S.S.P. Parkin, Prog Solid State Chem **39**, 391 (2011).

[50] H. Akai, Phys. Rev. Lett **81**, 3002 (1998).
[51] K. Sato, P.H. Dederichs, H. Katayama-Yoshida, Europhys.Lett **61(3)**, 403 (2003).
[52] A. H. Reshak, Z. Charifi, H. Baaziz, Eur. Phys. J. B **60**, 463 (2007).